A&A 558, A112 (2013)
DOI: 10.1051/0004-6361/201321898

Astronomy & Astrophysics

Laboratory rotational spectra of the dimethyl ether ^{13}C-isotopologues up to 1.5 THz⋆

M. Koerber[1], S. E. Bisschop[2,3], C. P. Endres[1], M. Kleshcheva[1,⋆⋆], R. W. H. Pohl[4], A. Klein[4], F. Lewen[1], and S. Schlemmer[1]

[1] I. Physikalisches Institut, Universität zu Köln, Zülpicher Str. 77, 50937 Köln, Germany
e-mail: koerber@ph1.uni-koeln.de
[2] Centre for Star and Planet Formation, Natural History Museum of Denmark, Øster Voldgade 5-7, 1350 Copenhagen, Denmark
[3] Centre for Star and Planet Formation, Niels Bohr Institute, Juliane Mariesvej 30, 2100 Copenhagen Ø., Denmark
[4] Institut für Anorganische Chemie, Universität zu Köln, Greinstr. 6, 50939 Köln, Germany

Received 15 May 2013 / Accepted 29 August 2013

ABSTRACT

Context. Dimethyl ether is found in high abundance in the interstellar medium. Owing to its strong and dense spectrum throughout the entire microwave and terahertz regime, it contributes to the spectral confusion in astronomical line surveys. The great sensitivity of new observatories like ALMA enhances the need for reliable spectroscopic data, especially for isotopic species of abundant molecules. In addition, the study of the interstellar $^{12}C/^{13}C$ isotopic ratio can be used as a tracer of the formation process of a molecular species, and thus it gives insight into the chemical evolution of the observed region.
Aims. The interpretation of astronomical observations depends on the knowledge of accurate rest frequencies and intensities. The objective of this work is to provide spectroscopic data for the two ^{13}C-isotopologues of dimethyl ether in the vibrational ground state.
Methods. High-resolution rotational-torsional spectra of $^{12}CH_3O^{13}CH_3$ and $(^{13}CH_3)_2O$ have been measured in the laboratory covering frequencies up to 1.5 THz. The analysis is based on an effective rotational Hamiltonian for molecules with two large-amplitude motions.
Results. Predictions of the complete ground state rotational spectrum of dimethyl ether-$^{13}C_1$ and -$^{13}C_2$ up to 2 THz are presented with accuracies better than 1 MHz. Based on the laboratory work, transitions of $^{12}CH_3O^{13}CH_3$ dimethyl ether have been detected for the first time in a large submillimeter line survey of the high-mass star forming region G327.3-0.6 performed with the APEX telescope.

Key words. molecular data – methods: laboratory – ISM: molecules – ISM: abundances – astrochemistry

1. Introduction

Dimethyl ether (DME) is an asymmetric top molecule with a relatively strong permanent dipole moment of $\mu = 1.302(10)$ D (Blukis et al. 1963). Its rotational spectrum is complicated by large-amplitude internal motion of both methyl groups interacting with the overall rotation of the molecule. This causes a splitting of each rotational level into torsional substates. Therefore DME exhibits a strong and dense spectrum throughout the entire microwave and terahertz regime that is relevant for astronomical observations. In addition, DME is known to be a prominent molecule in star forming regions that contributes to spectral line confusion in line surveys of these regions. First interstellar detection of DME was in the Orion nebula as reported by Snyder et al. (1974). Identification of DME in spectra of numerous high-mass star forming regions followed (e.g., Sutton et al. 1995; Nummelin et al. 1998, 2000). DME is detected as well in low-mass star forming regions (e.g., Cazaux et al. 2003; Jørgensen et al. 2005; Bacmann et al. 2012; Persson et al. 2012). The latest generation of telescopes like the Atacama Large Millimeter Array (ALMA) enhance the need for accurate prediction of transition frequencies in the terahertz region. Owing to the increased sensitivity of these observing facilities predictions are also required for isotopologues and vibrationally excited states of prominent molecules like DME.

Despite its abundance in star forming regions, the interstellar formation process of DME (CH_3OCH_3) has remained unclear up to now. Peeters et al. (2006) concluded that gas-phase synthesis via self-methylation of methanol ($CH_3OH_2^+ + CH_3OH \rightarrow CH_3OCH_4^+ + H_2O$) is the most efficient formation route for DME. Current gas-grain models (e.g., Garrod & Herbst 2006) assume that the surface reaction $CH_3 + CH_3O \rightarrow CH_3OCH_3$ is the most likely surface formation route in warm dense regions. They predict strong variations in the DME abundance during the evolutionary stage of a protostar with strong coupling of gas-phase and grain-surface chemistry (Garrod et al. 2008). However, the utility of DME as a "chemical clock" for the post-evaporation phase lies in the assumption that it is only formed from methanol (Peeters et al. 2006). Extensive modeling of the CH_3OCH_3 emission in the high-mass star forming region G327.3-0.6 (Bisschop et al. 2013) suggests that the gas-phase formation mechanism is dominant, but that a fraction greater than 5% of DME is likely formed on the surfaces of icy grains.

A more direct method of testing grain-surface formation of molecules has been proposed by Charnley et al. (2004) and is called "posterior isotopic labelling". The ion-molecule process $^{13}C^+ + {}^{12}CO \rightarrow {}^{13}CO + {}^{12}C^+$ with an exothermicity of 35 K

⋆ Full Tables 5 and 6 are only available at the CDS via anonymous ftp to cdsarc.u-strasbg.fr (130.79.128.5) or via http://cdsarc.u-strasbg.fr/viz-bin/qcat?J/A+A/558/A112
⋆⋆ Now: California Institute of Technology, Pasadena, CA 91125, USA.

is found to efficiently incorporate ^{13}C into CO at the expense of ^{12}C (Langer et al. 1984). This process is only efficient at 10 K. Therefore the atoms and molecules that accrete on cold grains and can participate in surface reactions to form complex molecules will be selectively fractionated in ^{13}C. If atom addition reactions to solid CO and HCO are the origin of organic molecules detected in hot molecular cores, these molecules should possess the same ^{12}C/^{13}C ratio as their parent molecules. Wirström et al. (2011) investigated the ^{12}C/^{13}C ratio of CO and methanol in various sources, and their results are consistent with the formation of methanol from hydrogenation of CO on grain surfaces. Further studies on ^{13}C-isotopologues of larger organic molecules like DME enable us to test astrochemical models and can provide important constraints on their evolutionary cycle.

Several laboratory studies of DME's main isotopologue ($^{12}CH_3)_2O$ have been performed over the past 50 years. Myers & Wilson (1960) applied group theory to derive symmetry properties, selection rules and spin statistical weights. In 1963 Blukis et al. recorded a few transitions of six isotopic species of DME to determine its structure and dipole moment. The potential barrier height to internal rotation was obtained by Durig et al. (1976) by measuring microwave transitions of the main isotopologue, as well as two deuterated forms of DME. First predictions for radio astronomy were provided by Lovas et al. (1979) in their review of all previous laboratory studies and new measurements of the vibrational ground state, which were later enhanced by Neustock et al. (1990). The most comprehensive work on the vibrational ground state of DME's main isotopologue was published by Groner et al. (1998), which was further expanded to higher frequencies by Endres et al. (2009). This work makes accurate predictions of the rotational spectrum possible up to 2.5 THz. The two lowest vibrationally excited states, $\nu_{11} = 1$ and $\nu_{15} = 1$, have also been studied by Endres et al. (in prep.), enabling a first astronomical detection of vibrationally excited DME by Bisschop et al. (2013). However, only very little is known about the ^{13}C-isotopologues of DME. Niide & Hayashi (2003) report some transition frequencies of DME-$^{13}C_1$ ($^{12}CH_3O^{13}CH_3$) below 50 GHz with maximum rotational quantum number $J = 8$. For DME-$^{13}C_2$ (($^{13}CH_3)_2O$), so far no rotational spectroscopic data are available.

The objective of the study reported in this paper is to provide accurate predictions of the rotational-torsional spectrum of both ^{13}C-isotopologues of DME up to terahertz frequencies to enable the astronomical detection of these species and in this way make it possible to study their abundances for astrochemical modeling. The paper is structured as follows. In Sect. 2 we present the symmetry properties of the dimethyl ether ^{13}C-isotopologues and summarize the theoretical approach to model their rotational spectra. Details on the experimental setup are given in Sect. 3. Using this setup, laboratory rotational spectra of $^{12}CH_3O^{13}CH_3$ and ($^{13}CH_3)_2O$ were recorded. Details on the experimental dataset and their analysis are given in Sect. 4. In Sect. 5 we conclude the laboratory analysis and discuss the implications for the astronomical detection of ^{13}C-isotopologues of dimethyl ether. Predictions based on the laboratory analysis have already led to a first detection of $^{12}CH_3O^{13}CH_3$ in the interstellar medium, which is also introduced in Sect. 5.

2. Theoretical model

DME is an asymmetric rotor close to the limiting case of a prolate symmetric top (Ray's parameter $\kappa = -0.92$). The permanent dipole moment of $\mu = 1.302(10)$ D lies parallel to the b principal inertial axis in the plane of symmetry. The two ^{13}C-isotopologues differ in their symmetry properties: Due to the identical methyl groups in ($^{13}CH_3)_2O$, this molecule has the same symmetry as the main isotopologue ($^{12}CH_3)_2O$. In the rigid rotor approximation both molecules belong to the C_{2v} point group. DME-$^{13}C_1$, $^{12}CH_3O^{13}CH_3$, does not have an axis of rotational symmetry, because its methyl groups are not equivalent. The point group symmetry of this isotopologue is C_s. However, the two methyl groups in DME perform large amplitude internal motions around the C-O bond with a barrier to internal rotation of 900 to 950 cm^{-1} (Durig et al. 1976; Groner & Durig 1977; Lutz & Dreizler 1978; Neustock et al. 1990; Niide & Hayashi 2004). The non-zero tunneling probability between the nine equivalent configurations of the molecule means that DME cannot be described as a rigid rotor. When taking the torsional motion into account, the symmetry of ($^{13}CH_3)_2O$ is given by the molecular symmetry group G_{36} (Longuet-Higgins 1963), whereas the symmetry of $^{12}CH_3O^{13}CH_3$ is described by the molecular symmetry group G_{18} (Bunker 1965). Each rotational energy level splits up into torsional substates, which are labeled by (00), (10), (01), (11), and (1-1)[1,2] rather than using the symmetry labels of the molecular symmetry group. In this labeling scheme, the notation for both isotopologues is equivalent, which avoids confusion. Pure rotational transitions only occur within each torsional substate. Owing to the equivalent methyl tops in ($^{13}CH_3)_2O$, the (10) and (01) states are degenerate and each rotational transition splits up into four torsional components[3] (00), (01), (11), and (1-1) with spin statistical weights 36, 64, 20, 16 for $ee - oo$ transitions and 28, 64, 12, 16 for $eo - oe$ transitions, respectively[4]. The rotational transitions of $^{12}CH_3O^{13}CH_3$ split up into five components[5] (00), (01), (10), (11), and (1-1). The spin statistical weight factors are 32, 32, 32, 16, and 16. Because of the interaction between the overall rotation and the torsional motion of the molecule, the torsional splitting of the ground state rotational levels is a function of the rotational quantum numbers J and K. The size of the splitting between the torsional substates (00), (01), and (11) is typically several megahertz, but the splitting between the substates (01) and (10), as well as (11) and (1-1), is significantly smaller and usually just a few kilohertz. Thus in Doppler limited measurements the splitting of transitions between these substates is not resolved in most cases. Usually a characteristic triplet is measured in the laboratory for rotational transitions of both DME isotopologues with the most intense torsional component (10)/(01) located between the two equally intense components (00) and (11)/(1-1).

To model the rotational-torsional levels of DME the effective rotational Hamiltonian `ERHAM` proposed by Groner was used. Details on the model are given in Groner (1997, 2012). In the following, only the very basic ideas are summarized. In the `ERHAM` approach, the basis for the wavefunctions is set up as products of the symmetric rotor eigenfunctions $|JKM\rangle$ and internal motion basis functions $|\nu\sigma_1(K)\sigma_2(-K)\rangle$. The quantum number ν characterizes the set of vibrational states, and σ_1, σ_2 are the

[1] The substates (10), (01), (11), and (1-1) are doubly degenerate.

[2] In the `ERHAM` code, (1-1) is called (12).

[3] In the commonly used notation referring to the $C_{3v}^- \otimes C_{3v}^+$ group introduced by Myers & Wilson (1960), the torsional states of ($^{13}CH_3)_2O$ are labeled (00)= AA, (01) = EE, (11) = AE, and (1-1) = EA (see also Dreizler 1961b).

[4] e (even) and o (odd) refer to the K_a, K_c labels of the energy states of an asymmetric rotor.

[5] Alternatively, the torsional levels for $^{12}CH_3O^{13}CH_3$ are labeled with (00) = AA, (01) = AE, (10) = EA, (11) = EE, and (1-1) = EE' using the $C_{3v}^{(1)} \otimes C_{3v}^{(2)}$ group (see Dreizler 1961a; Ohashi et al. 2004).

symmetry numbers labeling the torsional substates. The internal motion basis functions $|\nu\sigma_1(K)\sigma_2(-K)\rangle$ are derived from the solutions $|\nu\sigma_1(K_1)\sigma_2(K_2)\rangle$ of the torsional Hamiltonian H_I in the ρ-axis system, where $K_{1,2}$ are the projections of the overall angular momentum **J** onto the $\rho_{1,2}$-axes of the molecule. In the ERHAM approach, these solutions are not calculated explicitly. Groner makes use of their periodicity, and the internal motion basis functions are expressed in terms of localized functions with their spatial probability distribution localized in one of the nine minima of the potential. As a result, the matrix elements of the Hamiltonian become Fourier series whose coefficients are integrals of the localized functions. The benefit of this expansion is that every vibrational state ν is described by an individual set of Fourier coefficients without knowledge of the potential function. If the barrier to torsion is sufficiently high, the Fourier expansion quickly converges, which reduces the number of fitting parameters of this effective Hamiltonian significantly.

The effective Hamiltonian is finally given by

$$\langle JK'M\nu\sigma_1\sigma_2|H|JKM\nu\sigma_1\sigma_2\rangle = \sum_{K_1}\sum_{K_2} Y_{K'K}(K_1,K_2)\Sigma_0 + \sum_l \langle JK'M|R_l|JKM\rangle \Sigma_l. \quad (1)$$

The first term describes the matrix elements of the torsional energy, expressed as a two-dimensional Fourier series Σ_0. The matrix $Y_{K'K}(K_1,K_2)$ depends on the polar angles $\beta_{1,2}$ of the vectors $\rho_{1,2}$ to the principal inertial axes. It transforms the basis of the ρ-axis system to the principal axis system of the rotational operators. The second term of Eq. (1) contains the matrix elements of the rotational operators R_l in A-reduction multiplied by a two-dimensional Fourier series Σ_l. The Fourier series are given by

$$\Sigma_0 = \epsilon_{00} + 2\sum_{q>0}\left[\epsilon_{qq}\cos\alpha'_{qq} + \epsilon_{q-q}\cos\alpha'_{q-q} + \sum_{q'=-q+1}^{q-1}(\epsilon_{qq'}\cos\alpha'_{qq'} + \epsilon_{q'q}\cos\alpha'_{q'q})\right] \quad (2)$$

with

$$\alpha'_{qq'} = \tfrac{2\pi}{3}[q(\sigma_1-\rho K_1) + q'(\sigma_2-\rho K_2)] \quad (3)$$

and

$$\Sigma_l = T^{(\kappa)}_{l00} + 2\sum_{q>0}\left[T^{(\kappa)}_{lqq}\cos\alpha_{qq} + T^{(\kappa)}_{lq-q}\cos\alpha_{q-q} + \sum_{q'=-q+1}^{q-1}(T^{(\kappa)}_{lqq'}\cos\alpha_{qq'} + T^{(\kappa)}_{lq'q}\cos\alpha_{q'q})\right] \quad (4)$$

with $\kappa = K - K'$ and

$$\alpha_{qq'} = \tfrac{\pi}{3}[q(2\sigma_1 - \rho(K+K')) + q'(2\sigma_2 + \rho(K+K'))]. \quad (5)$$

Together with the internal motion parameter ρ and the polar angle β, the coefficients $\epsilon_{qq'}$ and $T^{(\kappa)}_{lqq'}$ of these Fourier series are the spectroscopic parameters. The Fourier coefficients with $q = q' = 0$ are the parameters describing the overall rotation (equivalent to the rotational parameters of molecules without torsional motion) and Fourier coefficients with $q > 0$ or $q' > 0$ arise from the interaction between internal and overall rotation. For equivalent internal rotors like in the case of $(^{13}CH_3)_2O$ the Fourier coefficients with qq' are equal to those with $q'q$, which simplifies the equations given above and further reduces the number of parameters needed to describe the molecule.

Table 1. Spectroscopic parameters for $^{12}CH_3O^{13}CH_3$ and $(^{13}CH_3)_2O$ in the vibrational ground state.

Parameter	$(^{13}CH_3)_2O$	$^{12}CH_3O^{13}CH_3$
ρ_1	0.215370(46)	0.21502(28)
ρ_2		0.21700(26)
β_1 (deg)	8.888(15)	9.093(61)
β_2 (deg)		8.731(65)
A (MHz)	38 439.90513(37)	38 615.74379(32)
B (MHz)	9538.241306(91)	9795.633147(78)
C (MHz)	8462.593602(87)	8673.668938(74)
Δ_J (kHz)	8.347491(98)	8.711394(99)
Δ_{JK} (kHz)	–27.22495(80)	–27.0258(11)
Δ_K (kHz)	342.1509(18)	341.9507(25)
δ_J (kHz)	1.582315(15)	1.676580(14)
δ_K (kHz)	–11.7538(18)	–12.7432(12)
Φ_J (Hz)	0.006679(30)	0.007265(32)
Φ_{JK} (Hz)	0.1177(14)	0.1279(12)
Φ_{KJ} (Hz)	–3.8858(52)	–3.9760(49)
Φ_K (Hz)	13.3577(86)	13.1835(64)
ϕ_J (Hz)	0.0034228(54)	0.0036653(49)
ϕ_{JK} (Hz)	0.2694(11)	0.29347(72)
ϕ_K (Hz)	1.976(48)	1.824(35)
l_K (mHz)	0.325(32)	0.504(46)
l_{JKK} (mHz)		0.0573(74)
Tunneling parameters		
ϵ_{01} (MHz)	–2.9387(14)	–2.9810(83)
ϵ_{10} (MHz)		–3.0083(83)
$[A-(B+C)/2]_{01}$ (kHz)	2.038(55)	1.49(64)
$[A-(B+C)/2]_{10}$ (kHz)		2.11(63)
$[(B+C)/2]_{01}$ (kHz)	–0.516(11)	–0.321(55)
$[(B+C)/2]_{10}$ (kHz)		–0.431(54)
$[(B-C)/4]_{01}$ (kHz)	–0.1612(75)	–0.1012(82)
$[(B-C)/4]_{10}$ (kHz)		–0.1012(82)*
$-[\Delta_J]_{01}$ (Hz)	0.2372(59)	0.1651(57)
$-[\Delta_J]_{10}$ (Hz)		0.1651(57)*
$-[\Delta_{JK}]_{01}$ (Hz)	–1.498(53)	–0.602(66)
$-[\Delta_{JK}]_{10}$ (Hz)		–0.602(66)*
$-[\Delta_K]_{01}$ (Hz)	2.078(35)	
$-[\delta_J]_{01}$ (Hz)	0.2138(75)	0.1732(71)
$-[\delta_J]_{10}$ (Hz)		0.1732(71)*
$-[\delta_K]_{01}$ (Hz)	0.623(43)	
$-[\delta_K]_{10}$ (Hz)		
$[\phi_J]_{01}$ (mHz)	–0.0512(21)	–0.0392(16)
$[\phi_J]_{10}$ (mHz)		–0.0392(16)*
σ_w	0.92	0.96

Notes. Subscript 1 refers to the internal rotor $^{13}CH_3$, and subscript 2 corresponds to $^{12}CH_3$. The non-tunneling Fourier parameters $T^{(\kappa)}_{l00}$ are given in the common notation for rotational constants. For tunneling parameters $T^{(\kappa)}_{lqq'}$ the notation $[\,]_{qq'}$ has been used with the corresponding non-tunneling parameters enclosed in the brackets. The standard deviation of the last two digits of the parameter is given in parentheses after the value.
(*) Parameter could not be fitted independently and is set to the same value as the corresponding $[\,]_{01}$ parameter.

The parameters of the effective Hamiltonian shortly introduced in this section (a detailed derivation is given in Groner 1997, 2012) were fitted to the experimental data in a least-squares analysis described in Sect. 4. A list of the parameters introduced to model the spectrum of the DME ^{13}C-isotopologues in the present investigation is given in Table 1.

3. Experimental details

Torsion-rotation spectra of DME-$^{13}C_1$ and -$^{13}C_2$ were recorded in Cologne in the millimeter and submillimeter regimes. Several

Table 2. Characterization of the different datasets used in the analysis of $^{12}CH_3O^{13}CH_3$.

Source	Frequency [GHz]	Number of transitions (lines)	Typ. exp. uncert. [kHz]	J_{max}	$K_{a,max}$	σ_{wrms}
Niide & Hayashi (2003)	8–34	36 (36)	50	7	2	1.13
Synthesizer	34–68	125 (89)	10	17	5	0.72
Tripler	75–120	389 (242)	20	31	8	0.83
Superlattice 3rd harm.	300–360	807 (439)	30	53	12	0.96
Superlattice 5th harm.	500–600	786 (289)	80	60	10	0.95
Superlattice 7th harm.	700–840	1236 (352)	110	53	14	1.01
Multiplier chain	1330–1500	1155 (123)	540	53	25	1.03

Table 3. Characterization of the different datasets used in the analysis of $(^{13}CH_3)_2O$.

Source	Frequency [GHz]	Number of transitions (lines)	Typ. exp. uncert. [kHz]	J_{max}	$K_{a,max}$	σ_{wrms}
Synthesizer	34–68	132 (106)	10	40	6	0.68
Tripler	75–120	596 (443)	20	55	18	0.98
Superlattice 3rd harm.	300–360	538 (358)	50	52	13	0.82
Superlattice 5th harm.	500–600	428 (227)	80	60	10	0.96
Superlattice 7th harm.	700–840	762 (223)	110	53	14	0.88
Multiplier chain	1330–1500	599 (78)	540	49	20	0.82

broadband scans were performed which cover the available frequency regions (see Tables 2 and 3) above 300 GHz completely. In addition, especially for the frequency regions below 300 GHz, numerous single scans were performed to measure spectra of single transitions with optimized signal-to-noise ratios. For frequencies up to 70 GHz, a commercial synthesizer was used as radiation source, and for frequencies up to 120 GHz, the synthesizer output was multiplied by a tripler. In both cases the signal was detected by a Schottky diode at room temperature. We used a single-pass absorption cell of 5 m length. For frequencies between 300 and 840 GHz, a combination of synthesizer and multiplier chain was used to produce high-power signals around 100 GHz, which were further multiplied by a superlattice device (for details on superlattice multipliers see Endres et al. 2007). Superlattice multipliers produce odd harmonics of the input frequency with the output power decreasing with each higher harmonic by about an order of magnitude. Transitions of DME in the frequency regimes of the 3rd, the 5th, and the 7th harmonic of the input frequency were assigned. To facilitate identification of spectra belonging to the 5th and the 7th harmonic, the spectra were measured three times using different dichroic filters to attenuate the radiation of the lower harmonics. The design and operation of dichroic filters is described in detail by Winnewisser et al. (1998). Higher frequencies up to 1.5 THz were accessed by combining the synthesizer with a multiplier chain producing the 108th harmonic of the input frequency. The setups for frequencies above 300 GHz used an InSb hot electron bolometer for detection and an absorption cell of 3 m length. To assure a frequency stability of the radiation sources of $\Delta\nu/\nu = 10^{-11}$, the synthesizer was locked to a reference signal of a rubidium atomic clock. For better signal-to-noise ratios, all spectra were recorded with $2f$-source modulation technique. The measurements were performed at room temperature with typical gas pressures between 15 and 50 μbar.

The sample of ^{13}C-DME was synthesized by slowly heating equal parts of ^{12}C- and ^{13}C-methanol with sulfuric acid. The evolving DME gas was condensed into a vacuum flask. The sample contained all possible carbon isotopic configurations $(^{12}CH_3)_2O$, $^{12}CH_3O^{13}CH_3$, and $(^{13}CH_3)_2O$ with proportion 1:2:1. In case of $(^{13}CH_3)_2O$ a pure sample was also synthesized from ^{13}C-methanol, which was used for the scans of single transitions. ^{13}C-methanol (at. 99%)[6] was used for the synthesis of DME without further purification.

4. Measured laboratory spectrum and analysis

A total of 1510 new lines were measured for $^{12}CH_3O^{13}CH_3$ and assigned to 4474 transitions. Energy levels including $J = 60$ and $K_a = 25$ were accessed. Previously published frequencies from Niide & Hayashi (2003) were included in the analysis for transitions up to 34 GHz with an uncertainty of 50 kHz. A number of 24 transitions between 35 and 48 GHz were remeasured with our spectrometer, and the new frequencies with lower uncertainty were added to the dataset. Deviations to the experimental frequencies given by Niide & Hayashi were between 10 kHz (experimental uncertainty) and 300 kHz. In the case of $(^{13}CH_3)_2O$, 1435 lines were measured and assigned to 3055 transitions including energy levels with $J = 60$ and $K_a = 20$. Assignments of this isotopologue in broad frequency scans were slightly complicated by the lower abundance of $(^{13}CH_3)_2O$ in the sample resulting in a lower signal-to-noise ratio compared to corresponding transitions of $^{12}CH_3O^{13}CH_3$. Details on the different datasets used in the analysis are given in Table 2 for $^{12}CH_3O^{13}CH_3$ and Table 3 for $(^{13}CH_3)_2O$. The analysis for both isotopologues includes a large number of Q- and R-branch transitions, as well as some P-branch and $\Delta K_a = 3$ transitions. To visualize and facilitate the assignments the AABS package by Kisiel was used. A brief description of the program package is given in Kisiel et al. (2005). The assignment of transitions was guided by predicted line positions and the intensity pattern that is in most cases characteristic. The predictions were improved iteratively during the assignments. Lines were not included in the analysis if the line profile and intensity were not reproduced well enough owing to a complicated structure or unknown blended transitions. The largest complications were due to level crossings affecting the order of nearly degenerate asymmetry levels with the same K_a. For some transitions, it was not possible to clearly define the asymmetric rotor labeling of the involved

[6] Purchased from Deutero GmbH, Kastellaun, Germany.

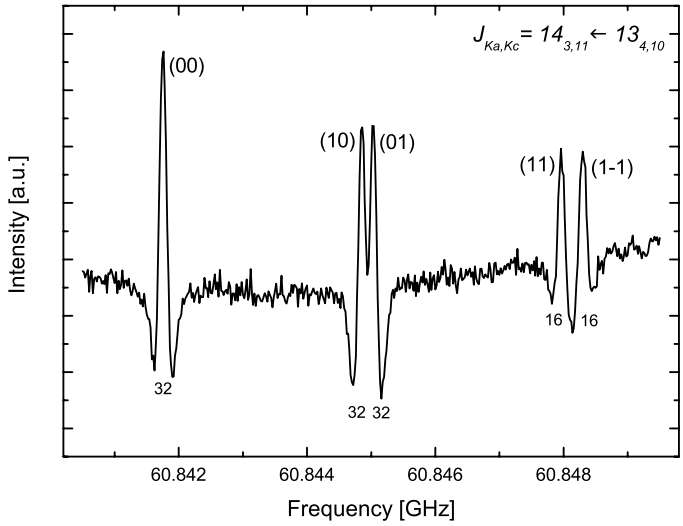

Fig. 1. Rotational transition $J_{Ka,Kc}$ = $14_{3,11}$−$13_{4,10}$ in the ground state of DME-$^{13}C_1$ at 60 GHz. The torsional splitting into the five substates (00), (10), (01), (11), and (1-1) is fully resolved. The spin statistical weights are denoted beneath each peak and are reflected by the relative intensities of the measured lines.

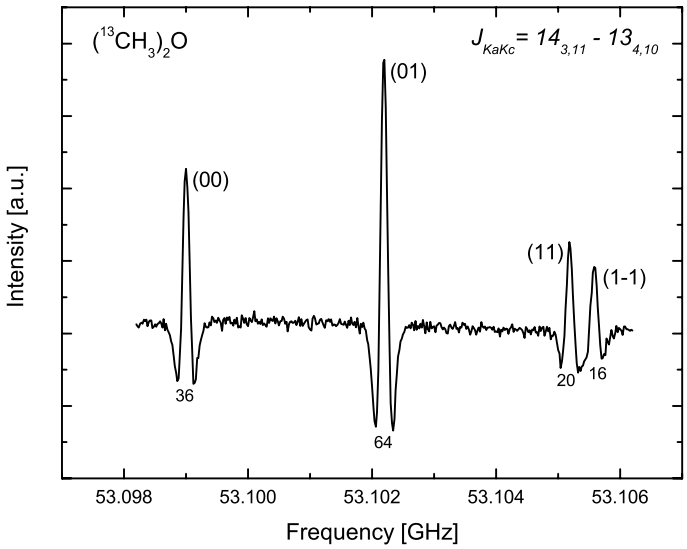

Fig. 2. Rotational transition $J_{Ka,Kc}$ = $14_{3,11}$−$13_{4,10}$ in the ground state of DME-$^{13}C_2$ at 53 GHz. The torsional splitting into the four substates (00), (01), (11), and (1-1) is fully resolved. The spin statistical weights are denoted beneath each peak and are reflected by the relative intensities of the measured lines.

states since the K_a-doublets were degenerate, and the labels frequently shifted due to numerical noise (see Groner 2012). These transitions are marked with an asterisk in the linelists, available at the CDS, given as supplementary material to this paper. However, thanks to the degeneracy of the energy levels, the transition frequencies are not affected by this.

In the lower frequency ranges, the line widths are small enough to completely resolve the torsional splitting into five substates (00), (01), (10), (11), and (1-1) in the case of DME-$^{13}C_1$ (four substates (00), (01), (11), and (1-1) in the case of DME-$^{13}C_2$ with two equivalent rotors). More than 250 transitions with at least partially resolved torsional splitting were recorded that access energy levels with J = 52 and K_a = 8. Pure rotational transitions only occur within a specific torsional substate. In most cases a characteristic pattern of three lines is observed for both isotopologues with blending of the substates (01) and (10), as well as (11) and (1-1). Transitions with completely resolved torsional splitting are shown in Fig. 1 for $^{12}CH_3O^{13}CH_3$ and in Fig. 2 for ($^{13}CH_3$)$_2$O. The spin statistical weights given in the figures are reflected well in the relative intensities of the lines recorded. These transitions provide valuable information on the torsional splitting of energy levels, because at higher frequencies the Doppler width of lines usually becomes too large to resolve the splitting. Therefore the dataset includes a large number of blended transitions. In the least-squares fit, the assigned frequency for a blended transition is weighted with its relative intensity compared to the other components of the spectral line. The intensities were taken from predictions using a dipole moment of μ = 1.302 D. Although systematic errors associated with improper intensity predictions cannot be fully excluded and could result in incorrect description of the torsional splitting, comparison of simulated and measured spectra indicates no obvious problems. As an example, Fig. 3 shows the torsional splitting for Q-branch transitions with K_a = 6 − 5 and K_c = J − K_a + 1. The experimental values agree nicely with the calculated transition frequencies within the given experimental uncertainties.

The least-squares analysis of all assigned transitions was performed using the computer program ERHAM (Groner 1997) based

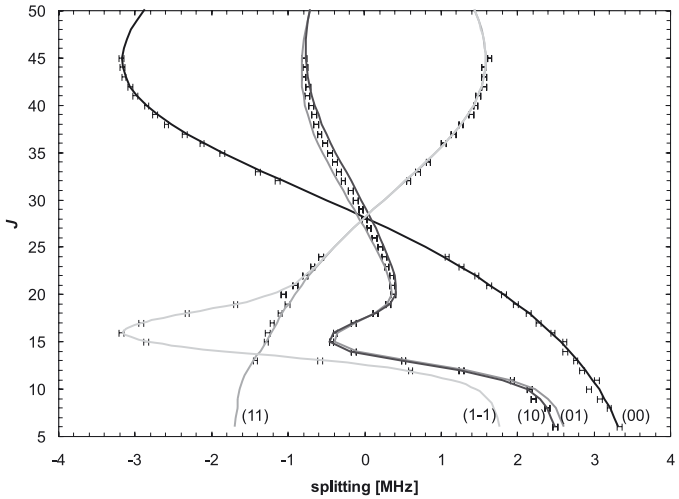

Fig. 3. Torsional splitting of Q-branch transitions with K_a = 6−5 and K_c = J − K_a + 1 in the vibrational ground state of DME-$^{13}C_1$. The solid lines connect predicted transitions belonging to the same torsional substate. Experimental data are shown as errorbars. The splitting displayed is the difference between the transition frequency observed or predicted and the frequency derived if all tunneling parameters are neglected.

on the effective Hamiltonian given in Sect. 2. As starting values for the fitting procedure, the values published for the main isotopologue by Endres et al. (2009) were taken. Just the rotational constants A, B, C, and the quartic centrifugal distortion parameters Δ_J, Δ_{JK}, Δ_K, δ_J, and δ_K were scaled to account for the effect of isotopic substitution on the moments of inertia. To find the best parameter set for the model to fit the assigned experimental transition frequencies, at first only transitions with low K values were fitted with an appropriate set of parameters. Successively, the range of K values in the fit was increased, and additional parameters were included to reproduce the assigned transitions within their experimental uncertainties. The spectroscopic parameters for $^{12}CH_3O^{13}CH_3$ and ($^{13}CH_3$)$_2$O obtained

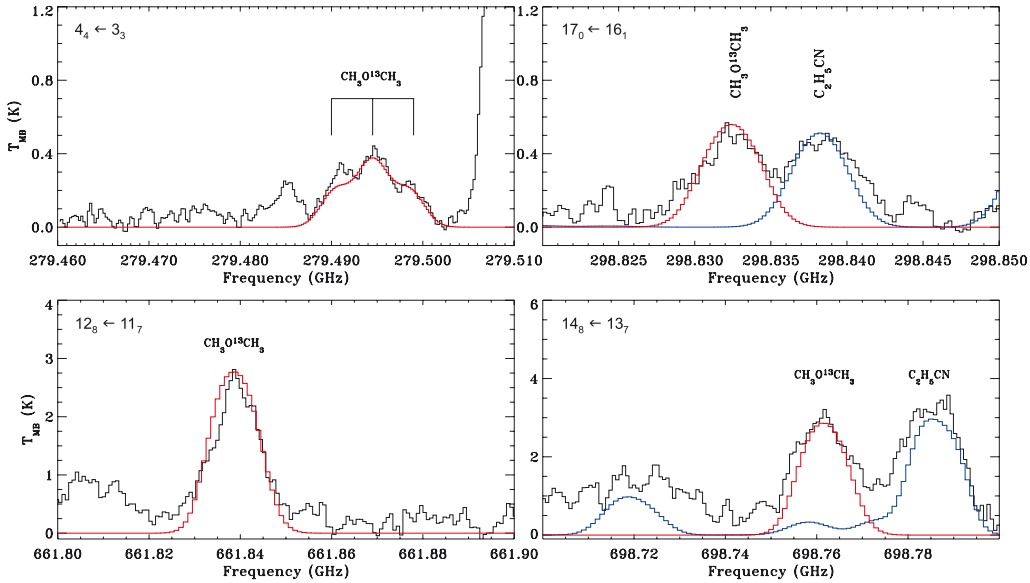

Fig. 4. Detail of the APEX line survey towards the hot core G327.3-0.6. The observed spectrum is depicted in black, and the model for $^{12}CH_3O^{13}CH_3$ is overplotted in red. The general model including transitions of all previously identified molecules is given in blue. The spectroscopic assignment of transitions of DME-$^{13}C_1$ is given in the upper left of each individual panel. The asymmetry splitting and the torsional splitting of transitions is not resolved in these lines, except for the first panel, in which the torsional splitting into three components is indicated.

from this analysis are given in Table 1. Only Fourier parameters with $q, q' = 0$ and $q, q' = 1$ were needed to describe the spectrum. In case of $^{12}CH_3O^{13}CH_3$ Fourier parameters with qq' and $q'q$ occur due to the two non-equivalent rotors. However, it was not possible to fit most of these parameters independently. For this reason, parameters with $q'q$ were set to the same value as the corresponding parameter with qq'. It is expected that the difference between the values of these parameters should be very small because the two rotors in $^{12}CH_3O^{13}CH_3$ are very similar given that the two different carbon isotopes are located almost on the axes of internal rotation. When including new parameters in the fit, several possible coefficients were tested, and those were kept that have the largest effect on the reduced standard deviation of the fit. A discussion of the differences in the spectroscopic parameters for all three carbon isotopologues of DME is given in detail in the Ph.D.-Thesis by Koerber (2012).

5. Conclusion and discussion

New laboratory data on DME-$^{13}C_1$ and -$^{13}C_2$ were recorded from 34 GHz up to 1.5 THz. For $^{12}CH_3O^{13}CH_3$, the existing data by Niide & Hayashi (2003) were substantially extended, and for $(^{13}CH_3)_2O$ the first rotational spectroscopic data are presented. Transitions involving energy levels up to $J = 60$ and $K_a = 25$ ($K_a = 20$, respectively) were analyzed and fitted to experimental uncertainty using the ERHAM effective rotational Hamiltonian for molecules with two large-amplitude motions.

Based on the laboratory analysis reported in this paper, transitions of DME-$^{13}C_1$ were detected in interstellar space for the first time as part of a large unbiased line-survey toward the chemically rich, high-mass hot core G327.3-0.6 (Bisschop et al., in prep.) performed with the APEX telescope (Güsten et al. 2006). The resulting bandwidth was 1.9 GHz covered per setting in the 230, 290, and 345 GHz frequency windows, and 2.8 GHz at 690 and 810 GHz. For more details on the observations, see Bisschop et al. (2013) and references therein.

In this survey, more than 100 previously unassigned emission lines correspond to rotational transitions of $^{12}CH_3O^{13}CH_3$.

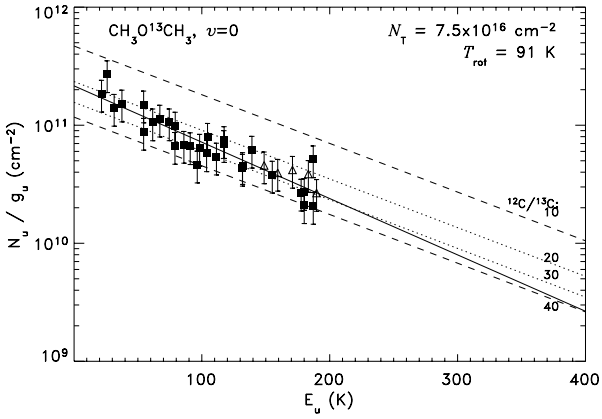

Fig. 5. Rotational diagram for $CH_3O^{13}CH_3$ corrected for the optical depth. The data has been corrected for the dust optical depth, as well as the modeled line emission from other species. The filled squares (■) represent transitions detected with SHeFI in the 230, 290, and 345 GHz windows, and the open triangles (△) indicate CHAMP$^+$ data. The solid line shows the fit to the combined SHeFI and CHAMP$^+$ data, the dotted lines the fit to the main isotopologue by Bisschop et al. (2013) corrected for a $^{12}C/^{13}C$ ratio of 20 and 30, and the dashed lines a $^{12}C/^{13}C$ ratio of 10 and 40.

Table 4. Resulting best fit for the *myXCLASS* model.

θ ($''$)	$T_{\rm rot}$ (K)	N_T (cm^{-2})	ΔV (km s^{-1})
2.6(0.2)	100(5)	6.0×10^{16}(0.5)	4(0.3)
3.2(0.2)	80(5)	3.0×10^{15}(0.5)	4(0.3)

Notes. The estimated uncertainties of the different parameters are given in parentheses.

An example of four transitions at frequencies around 300 GHz and 600 GHz, respectively, is given in Fig. 4. In Fig. 5 the Boltzmann diagram is shown for the 41 unblended features detected for $CH_3O^{13}CH_3$, and the fits for the main isotopologue

Table 5. Excerpt from the experimental transition frequencies of $^{12}CH_3O^{13}CH_3$.

Tors. substate $\sigma_1\sigma_2$	J'	K'_a	K'_c	J''	K''_a	K''_c	Frequency (MHz)	Rel. weight in blend	Uncert. (MHz)	Obs.-calc. (MHz)	Weighted obs.-calc. for set of blends (MHz)
00	8	1	8	7	2	5	34 549.9764	0	0.01	0.001	
10	8	1	8	7	2	5	34 552.5450	0.5	0.01	0.0313	
01	8	1	8	7	2	5	34 552.5450	0.5	0.01	–0.0304	0.0005
1–1	8	1	8	7	2	5	34 555.1114	0.5	0.01	0.005	
11	8	1	8	7	2	5	34 555.1114	0.5	0.01	–0.0096	–0.0023
11	4	1	3	4	0	4	35 383.7468	0.5	0.01	0.0022	
1–1	4	1	3	4	0	4	35 383.7468	0.5	0.01	0.0007	0.0014
01	4	1	3	4	0	4	35 384.7105	0.5	0.01	0.0126	
10	4	1	3	4	0	4	35 384.7105	0.5	0.01	–0.009	0.0018
00	4	1	3	4	0	4	35 385.6620	0	0.01	–0.0101	
00	13	3	11	12	4	8	35 727.7498	0	0.01	–0.0012	
10	13	3	11	12	4	8	35 730.7270	0	0.01	–0.0166	
01	13	3	11	12	4	8	35 730.8599	0	0.01	–0.0066	
1–1	13	3	11	12	4	8	35 733.5068	0	0.01	–0.0206	
11	13	3	11	12	4	8	35 734.1965	0	0.01	0.0025	

Notes. The full experimental linelist is available at the CDS.

Table 6. Excerpt from the experimental transition frequencies of $(^{13}CH_3)_2O$.

Tors. substate $\sigma_1\sigma_2$	J'	K'_a	K'_c	J''	K''_a	K''_c	Frequency (MHz)	Rel. weight in blend	Uncert. (MHz)	Obs.-calc. (MHz)	Weighted obs.-calc. for set of blends (MHz)
11	4	1	3	4	0	4	35178.2700	0.64	0.01	–0.0006	
1–1	4	1	3	4	0	4	35178.2700	0.36	0.01	–0.0021	–0.0011
01	4	1	3	4	0	4	35179.2100	0	0.01	0.0013	
00	4	1	3	4	0	4	35180.1400	0	0.01	–0.006	
11	5	1	4	5	0	5	38315.2800	0.43	0.01	0.0026	
1–1	5	1	4	5	0	5	38315.2800	0.57	0.01	0.0018	0.0021
01	5	1	4	5	0	5	38316.2600	0	0.01	0.0028	
00	5	1	4	5	0	5	38317.2300	0	0.01	–0.0067	
11	6	1	5	6	0	6	42298.5300	0.64	0.01	0.0038	
1–1	6	1	5	6	0	6	42298.5300	0.36	0.01	0.0033	0.0036
01	6	1	5	6	0	6	42299.5600	0	0.01	0.0017	
00	6	1	5	6	0	6	42300.5900	0	0.01	–0.0001	

Notes. The full experimental linelist is available at the CDS.

are overplotted for different ratios. This comparison shows that the abundance ratio for the $^{12}C/^{13}C$ dimethyl ether isotopologues lies between 20 and 30. The intensities of the blended transitions are consistent with our expectations based on the unblended transitions in combination with the other species contributing to these line blends.

The model for the $CH_3O^{13}CH_3$ emission has been determined with the *myXCLASS* program[7] (Comito et al. 2005). The program assumes the source to be isothermal and line shapes to be Gaussian. The $CH_3O^{13}CH_3$ transitions were best fit with the same two-component model as for its main isotopologue, but with a lower abundance by a factor of ~25. The source size (θ), rotational temperature ($T_{\rm rot}$), source averaged column density (N_T), and linewidth (ΔV) are given in Table 4. The source sizes were assumed to be the same as for the main isotopologue, since none of the $CH_3O^{13}CH_3$ transitions were found to be optically thick, and the source size could thus not be determined independently.

The $^{12}C/^{13}C$ abundance ratio for DME in this interstellar source of about 25 ± 5 indicates the gas-phase formation route to be dominant for DME. Both carbon atoms are equivalent in DME, and thus its $^{12}C/^{13}C$ abundance ratio is expected to be less than that of, say, methanol (which is around 50) if gas-phase processes are significant for the formation of DME. A detailed analysis will be given in an upcoming paper by Bisschop et al. (in prep.).

The laboratory analysis enables us to predict the complete ground state rotational spectra of DME-$^{13}C_1$ and -$^{13}C_2$ up to 2 THz. For transitions not exceeding the range of quantum numbers covered by the laboratory analysis presented in this paper, the accuracy is expected to be better than 1 MHz. In astronomical sources the main isotopologue of DME in its vibrational ground state has been detected at various rotational temperatures; e.g., in Orion KL rotational temperatures of 89 K (Schilke et al. 1997) and 360 K (Schilke et al. 2001) were reported. For an intermediate rotational temperature of 200 K, the most intense transitions for the ^{13}C-isotopologues are found between 750 GHz and 900 GHz with quantum numbers J and K_a in the range of 10−13. Therefore the data presented here for the two ^{13}C-isotopologues of DME offer a very reliable basis for astronomical applications and makes an interstellar detection of these isotopologues possible in other line-rich hot core sources. The range of predictions and their accuracy also fulfill the requirements for ALMA with its exceptional sensitivity and spatial resolution, which will also be able to probe weaker

[7] http://www.astro.uni-koeln.de/projects/schilke/XCLASS

transitions. With ALMA it may even be possible to detect transitions of DME-$^{13}C_2$. Transitions within excited vibrational states of DME-$^{13}C_1$ will also play a role in the ALMA spectra, since at 200 K a fraction of about 15% and 11% of the molecules is excited to the two lowest torsional states. Therefore we will further extend our laboratory studies of the ^{13}C-isotopologues of DME to torsional excited states. The list of measured frequencies of the laboratory study presented here is given as supplementary material of this paper lodged at the CDS. Tables 5 and 6 show a preview of the data stored at the CDS. Predictions are available through the Cologne Database for Molecular Spectroscopy (CDMS[8], Müller et al. 2001, 2005), together with the values of the partition function for different temperatures.

Acknowledgements. We thank the Deutsche Forschungsgemeinschaft (DFG) for financial support through research grants "Molecular Complexity", contract no. SCHL341/10-1, and the Collaborative Research Council 956, sub-project B3.

References

Bacmann, A., Taquet, V., Faure, A., Kahane, C., & Ceccarelli, C. 2012, A&A, 541, L12
Bisschop, S. E., Schilke, P., Wyrowski, F., et al. 2013, A&A, 552, A122
Blukis, U., Myers, R. J., & Kasai, P. H. 1963, J. Chem. Phys., 38, 2753
Bunker, P. R. 1965, Mol. Phys., 9, 257
Cazaux, S., Tielens, A. G. G. M., Checcarelli, C., et al. 2003, ApJ, 593, L51
Charnley, S. B., Ehrenfreund, P., Millar, T. J., et al. 2004, MNRAS, 347, 157
Comito, C., Schilke, P., Philips, T. G., et al. 2005, ApJS, 156, 127
Dreizler, H. 1961a, Z. Naturforsch. A, 16, 1354
Dreizler, H. 1961b, Z. Naturforsch. A, 16, 477
Durig, J. R., Li, Y. S., & Groner, P. 1976, J. Mol. Spectrosc., 62, 159
Endres, C. P., Lewen, F., Giesen, T. F., et al. 2007, Rev. Sci. Instr., 78, 043106
Endres, C. P., Drouin, B. J., Pearson, J. C., et al. 2009, A&A, 504, 635
Garrod, R. T., & Herbst, E. 2006, A&A, 457, 927
Garrod, R. T., Widicus Weaver, S. L., & Herbst, E. 2008, ApJ, 682, 283
Groner, P. 1997, J. Chem. Phys., 107, 4483
Groner, P. 2012, J. Mol. Spectrosc., 278, 52
Groner, P., & Durig, J. R. 1977, J. Chem. Phys., 66, 1856
Groner, P., Albert, S., Herbst, E., & De Lucia, F. C. 1998, ApJ, 500, 1059
Güsten, R., Nyman, L. A., Schilke, P., et al. 2006, A&A, 454, L13
Jørgensen, J. K., Bourke, T. L., Myers, P. C., et al. 2005, ApJ, 632, 973
Kisiel, Z., Pszczolkowski, L., Medvedev, I. R., et al. 2005, J. Mol. Spectrosc., 233, 231
Koerber, M. 2012, Ph.D. Thesis, Universität zu Köln
Langer, W. D., Graedel, T. E., Frerking, M. A., & Armentrout, P. B. 1984, ApJ, 277, 581
Longuet-Higgins, H. C. 1963, Mol. Phys., 6, 445
Lovas, F. J., Lutz, H., & Dreizler, H. 1979, J. Phys. Chem. Ref. Data, 8, 1051
Lutz, H., & Dreizler, H. 1978, Z. Naturforsch. A: Phys. Sci, 33, 1498
Müller, H. S. P., Thorwirth, S., Roth, D. A., & Winnewisser, G. 2001, A&A, 370, L49
Müller, H. S. P., Schlöder, F., Stutzki, J., & Winnewisser, G. 2005, J. Mol. Struct., 742, 215
Myers, R. J., & Wilson, Jr., E. B. 1960, J. Chem. Phys., 33, 186
Neustock, W., Guarnieri, A., Demaison, J., & Wlodarczak, G. 1990, Z. Naturforsch. A: Phys. Sci., 45, 702
Niide, Y., & Hayashi, M. 2003, J. Mol. Spectrosc., 220, 65
Niide, Y., & Hayashi, M. 2004, J. Mol. Spectrosc., 223, 152
Nummelin, A., Bergman, P., Hjalmarson, A., et al. 1998, ApJS, 117, 427
Nummelin, A., Bergman, P., Hjalmarson, A., et al. 2000, ApJS, 128, 213
Ohashi, N., Hougen, J. T., Suenram, R. D., et al. 2004, J. Mol. Spectrosc., 227, 28
Peeters, Z., Rodgers, S. D., Charnley, S. B., et al. 2006, A&A, 445, 197
Persson, M. V., Jørgensen, J. K., & van Dishoeck, E. F. 2012, A&A, 541, A39
Schilke, P., Groesbeck, T. D., Blake, G. A., & Phillips, T. G. 1997, ApJS, 108, 301
Schilke, P., Benford, D. J., Hunter, T. R., Lis, D. C., & Phillips, T. G. 2001, ApJS, 132, 281
Snyder, L. E., Buhl, D., Schwartz, P. R., et al. 1974, ApJ, 191, L79
Sutton, E. C., Peng, R., Danchi, W. C., et al. 1995, ApJS, 97, 455
Winnewisser, C., Lewen, F., & Helm, H. 1998, Appl. Phys. A, 66, 593
Wirström, E. S., Geppert, W. D., Hjalmarson, A., et al. 2011, A&A, 533, A24

[8] http://www.cdms.de